View metadata, citation and similar papers at core.ac.uk

brought to you by CORE

provided by Elsevier - Publisher Connector

Available online at www.sciencedirect.com

SciVerse ScienceDirect

Procedia Environmental Sciences 13 (2012) 53 – 70

Procedia Environmental Sciences

The 18th Biennial Conference of International Society for Ecological Modelling

Development of a calculation method for blown sand movement above the barchan dunes using spatial analysis

He-Qiang Du [a*], Zhang Yang[b]

[a] *Cold and Arid Regions Environmental and Engineering Research Institute, Chinese Academy of Sciences, Lanzhou 730000, Gansu, China;*

[b] *College of Environment and Resources, Wuhan University, Wuhan 430079, China*

Abstract

Blown sand movement threatened the ecosystems severely in arid zones. The research on blown sand movement is an important component of the controlling blown sand hazard. In the present study, we developed a method that based on GIS-based spatial analysis to calculate the blown sand movement above the surface of a barchan dune. To do so, we sampled the diameters of sand grains, wind velocity and sand flux above the surface of a barchan dune in Taklimakan Desert. Interpolated the sand grain diameters and wind velocity by means of Kriging and Inverse Distance Weighting, respectively, we got the continuous distribution of sand grain diameters and wind velocity above this dune. Integrated these interpolated results, we computed the aerodynamic roughness length, the friction velocity and the sand flux by blown sand models. By this calculation method, the continuous distribution of the aerodynamic roughness length, the friction velocity and the sand flux were obtained. To test this calculation method, we compared these predicted data with the observed values. The tested results showed that the predicted results (the aerodynamic roughness length, the friction velocity and the sand flux) by this method are all satisfied except the sand flux above the dune's foot. We thought that the not enough accurately modeling result of sand flux above the dune's foot is caused by unsaturated sand flux was generated above there, and the models we used are all based the theory of saturated sand flux. Though cans not accurately modeling the sand flux above the dune's foot, this blown sand movement calculation approach is better than those traditional observation methods on the whole.

© 2011 Published by Elsevier B.V. Selection and/or peer-review under responsibility of School of Environment, Beijing Normal University. Open access under CC BY-NC-ND license.

Keywords: blown sand movement; spatial analysis; barchan dune; test results

* Corresponding author. Tel.: +86-0931-4967560; fax: +86-0931-4967555.
E-mail address: dilikexue119@163.com.

1878-0296 © 2011 Published by Elsevier B.V. Selection and/or peer-review under responsibility of School of Environment, Beijing Normal University. Open access under CC BY-NC-ND license. doi:10.1016/j.proenv.2012.01.005

1. Introduction

Blown sand movement threatened the ecosystems severely in arid zones. The study of blown sand movement is an important component of the controlling blown sand hazard. Observe and simulate the blown sand movement can provide a scientific foundation for defining reasonable programs, measures, and structures that can be used in sand-control engineering [1]. Since the British scholar Bagnold observed and experimented with sand fluxes in North Africa in the 1930s [2], scholars from around the world have studied blown sand movement, leading to the development of many empirical and physics-based theories and equations.

For example, Tsoar proved that the wind velocity decreases abruptly at the foot of the stoss slope using wind tunnel experiments and theoretical analysis [3]. Lancaster reported that the friction velocity decreased with increasing elevation along the stoss slope and decreased drastically at the crest of barchan dunes, but the wind velocity increased nonlinearly along the dunes' stoss side [4, 5]. Burkinshaw et al. concluded that the air flow would converge and accelerate above dunes, and the surface erosion would be increased by abrupt slopes, based on observations of the wind profiles during a dune's different evolutionary phases; Burkinshaw called these the nonequilibrium state, quasi-equilibrium state, and equilibrium state [6]. Wiggs noted the sand flux varied nonlinearly with dunes' height, and concluded that the erosion and deposition would reach their maximum values in the middle of the stoss slope and at the crest, respectively [7]. Through observed the wind velocity and sand flux above the surfaces of two mega-dunes, McKenna et al. found that the sand flux increased steadily from the foot to the crest of dunes and that the crest of the dunes was the most active position due to the continuous acceleration of air flow along the stoss slope [8]. Stam described the relationship between the friction stress and the erosion of the dunes' surface, and developed three dune evolution models which based on dynamical, analytical, and numerical, respectively [9]. Sauermann et al. studied the unsaturated sand flux along a barchan dune's stoss side and made a continuum model to calculate the unsaturated sand flux [10, 11].

Barchans are one of the most common forms of dune. They are known to exist in regions with limited sediment supply and unidirectional wind regimes [12]. Researchers have investigated the particle-size composition, wind profile, aeolian saltation cloud, dynamic processes that govern their evolution, depositional models, and many other aspects of barchans [13~18].

As spatial threory and technology has advanced, Remote sensing and Geographic Information Systems (GIS) have become been widely used in the study of blown sand movement [17~20]. However, these research were all emphasis on the relationship between the sand flux and migration in vast regions, and all of these study had no idear about the variation of blown sand movement above the different parts of a single barchan. In this situation, our study that based on GIS spatial analysis supplied a continuous distribution of aerodynamic roughness length, friction velocity and sand flux above a barchan dune and we believe it would supplement this problem.

For the perturbation of the landform, it is cost time and energy to simulate the aerodynamic roughness length, friction velocity and sand flux in traditional method, so some scholars have suggested that used the fixed point observation method to obtain the blown sand movement parameters above the dunes [21, 22]. This approach provides researchers with precise measurements at these points. However, this approach does not provide data for the entire dune and it can miss some important points where the values vary abruptly. In the present study, we used several blown sand movement calculation equations to calculate the aerodynamic roughness length, friction velocity and sand flux above a barchan dune in spatial analysis module of ArcGIS 9.2 working platform. We compared these predicted results with the observed values, and found that the predicted results are all satisfied except the sand flux above the dune's foot. This method can overcome the above mentioned deficiency of the traditional method that based on fixed observation points.

2. Overview of the study area

We selected a study area at the Tazhong Station, which is located in the center of the Taklimakan Desert (39°00′N , 83°40′E), Xinjiang province (Fig 1). This area has a typical arid temperate continental climate, with annual precipitation averaging less than 50 mm and evaporation values up to 3000 mm. The average relative humidity is 35% in July, and the minimum relative humidity decreases nearly to 0%. Summers could be extremely hot, with the maximum temperature reaching 50°C, whereas winter temperatures are low, reaching a minimum of -20°C. Strong winds blow during 7 months in one year. The maximum wind velocity reaches 30 $m \cdot s^{-1}$, and the main wind direction is from the northeast [23].

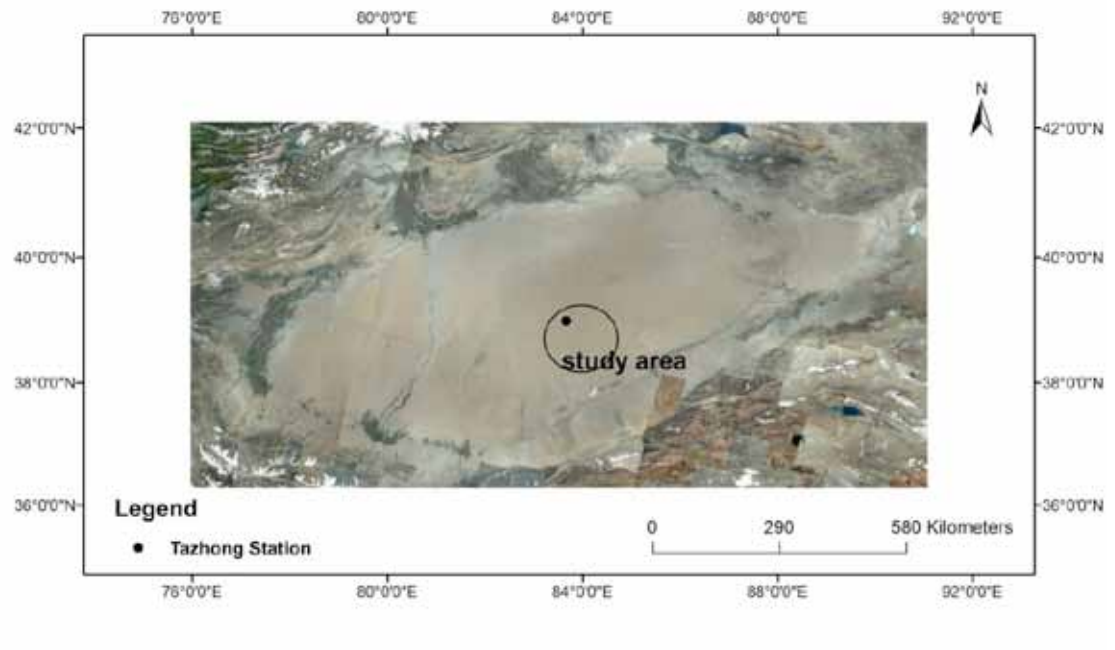

Fig. 1. Google earth image of the center of the Taklimakan Desert. The circinal area is our studied area

High composite longitudinal dunes are widely distributed in the study area, with their long axis running between N50°E to N56°E, and their heights ranging from 60 to 80 m. The cross-sections of the longitudinal dunes are asymmetrical, with southeast side extending farther than the northwest. Between the longitudinal dunes are flat sandy ground with width of 1 to 2 km. Scattered barchans with height of 1 to 2 m are distributed in the flat ground between the longitudinal dunes. These dunes are oriented with their slip face facing S70°W, with a slip face slope of about 32° and a stoss slope of about 11°. These isolated barchans are very typical of this class of dunes. The main particles (about 94%) that make up these dunes are fine and very fine sands (0.09 mm ~ 0.11 mm).

We selected a single barchan dune for detailed study. We got the height profile h(x) of stoss slope and ridge line by measuring the change in height every 0.2 m form the crest to the foot of stoss slope, from the crest to the slip face and from the crest to the horns. This dune was 1.3 m tall, 6.8 m wide, and had a stoss slope that was 5.6 m long. We characterized this dune by sampling the sand grain diameters, wind velocity, and sand flux above the dune.

3. Study method

3.1. Sampling the particle size

In our sampling, we defined the following geometry: The flat sands around the barchan dune were treated as the *x*–*y* plane, with the foot of stoss slope representing the origin of a rectangular Cartesian coordinate system. The downwind axis of the dune represents the *x*-axis, the crosswind axis of the dune represents the *y*-axis, and the relative elevation of this dune above the *x*–*y* plane represents the *z*-axis (Fig 2a).

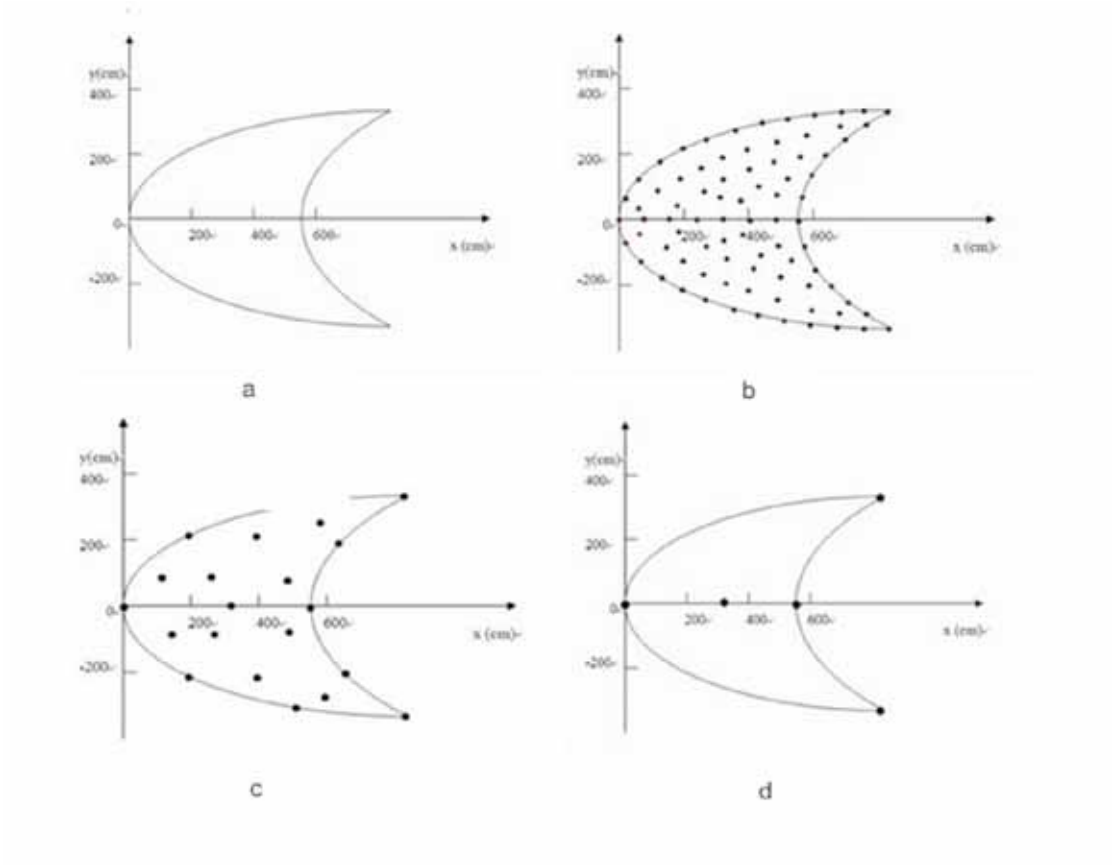

Fig. 2. (a) Illustration of the barchan dune's geometry in the rectangular Cartesian coordinate system; (b) Distribution of sand particle size samples above the dune; (c) Distribution of wind velocity samples above the dune; (d) Distribution of sand flux samples above the dune.

Within this coordinate system, we sampled the sand grain diameters above the barchan dune. The sampling points were approximately equally distributed along the slip face, the crest of this dune, the stoss slope, the dune's foot, the two horns of this dune, and in the flat ground surrounding the dune. To obtain these samples, we used quadrats with an area of 5×5 cm, and a depth of 5 to 10 cm. We obtained a total of 81 samples. The coordinates of each of the sample points was given an (x, y, z) coordinate in the Cartesian coordinate system (Fig 2b).

3.2. Wind velocity and sand flux collecting

Perturbations caused by the topography make the wind velocity to increase nonlinearly from the dune's foot to the crest [24]. The sand transport occurs within a shear-stress layer in which interactions between the wind and the bed take place. Hunt et al. note that the height (Z) of the shear-stress layer for wind blowing over a hill (or a dune) can be obtained implicitly through the following equation[25]:

$$Z_T = \frac{2k^2 L}{\ln Z_T / z_0} \tag{1}$$

where, Z_T denotes the height of the shear stress layer; k=0.4(Von Karman's constant); L = 3.5 m, and represents the characteristic length of the dune, which is measured from the half height of the stoss side to the crest, as defined by Hunt et al.[25]; and z_0 represents the bed roughness length, which equals d/30, where d is the average sand grain diameter (0.01 cm) [2]. Based on this relationship, we calculated the height of the shear-stress layer as $Z_T \approx 60$ cm. On this basis, we placed anemometers (as described below) at a height of 30 cm so that they would be well inside the shear-stress layer.

We used two anemometers to observe the wind velocity inside the shear-stress layer. The observation method as follow: first, we selected an area of flat ground about 100 m upwind of the dune's foot to place the reference anemometer that would be used to normalize the wind velocity data above the dune. Every sampling period lasted 10 minutes, and we recorded the average wind velocity (v_i) for that period. Seconde, we installed the other anemometer at 20 points successively, where we sampled the particle sizes in the surface of the dune. The sampling points were homogeneously distributed among the dune's foot, the stoss slope, the crest, and the both horns (Fig 2c). The samples (v_{ixy} for period i at coordinates x and y) were also recorded as the average values in a period of 10 minutes. We collected a total of 20 samples at each point at intervals of 10 min over a period of 200 min.

At the beginning of the first time of wind velocity observed, we also installed stagewise-multiaperture sand collectors which has 30 channels (each channel's area is 1 cm × 1 cm) for collecting sand at the foot of the stoss slope, at the middle part of the stoss slope, at the dune's crest, and at both horns (Fig 2d). It was collected during the same 10 minutes used to check the sand flux model and the coordinates of these data were recorded. We defined these values as the sand flux (o_x) at point (x, y).

3.3. Data processing

3.3.1. Particle size data pracessing

We used these particle-size values to interpolate particle sizes between the sampling points using the Kriging method due to this method takes anisotropism into consideration. Geostatistical minds reflected fully in this method, which provided a optimal tactics, and a linear unbbiased estimation of the values of given spots.

The interpolation method of Kriging can be computed as:

$$\hat{Z}(x_0) = \sum_{i=1}^{n} \lambda_i Z(x_i) \qquad (2)$$

where, $\hat{Z}(x_0)$ is the predicted value of particle size at the point x_0; n is the number of sampling points around the predicted point that is used in computing the predicted value; λ is the weight factor that decreases with increasing distance between the sample points and the predicted points; and $Z(x_i)$ is the observed mean particle size at sample point i.

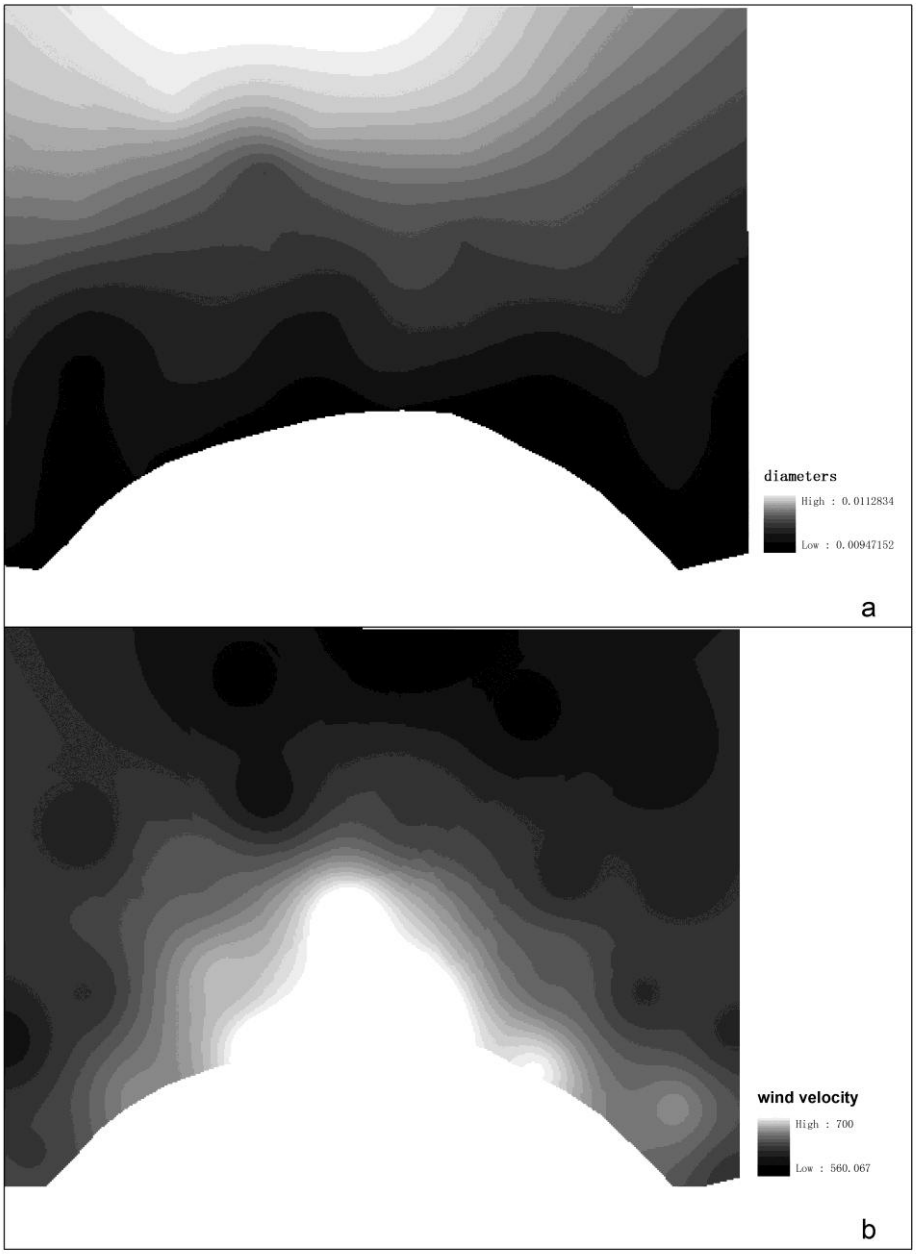

Fig. 3. Distribution of particle diameters and wind velocity above the surface of the barchan dune (a. Distribution of particle diameters above the dune's surface; b. Distribution of wind velocity above the dune's surface)

In the constraint condition of $\sum_{i=1} \lambda_i = 1$, the chosen of λ could ensure that the prediction is unbiased and optimum. That is:

$$E[\hat{Z}(x_0) - Z(x_0)] = 0 \quad (3)$$

and

$$E[\hat{Z}(x_0) - Z(x_0)]^2 = \min \quad (4)$$

where, $Z(x_0)$ is the truth value at the point of x_0.

This interpolation was performed using the Geostatistical Analyst module of the ArcGIS 9.2 software (ESRI, Redlands, Calif.). In this approach, we calculated a graph of the diameter distribution of the particles with 2×2 cm grids (Fig 3a). To unify the dimensions, we used the following relationship to transform the φ unit into cm:

$$d = (d_0 \times 2^{1\varphi}) / 10 \quad (5)$$

where, d is the mean particle diameter (cm), φ is the Krumbein phi value, and d_0 is the base number of particle diameter (1 mm).

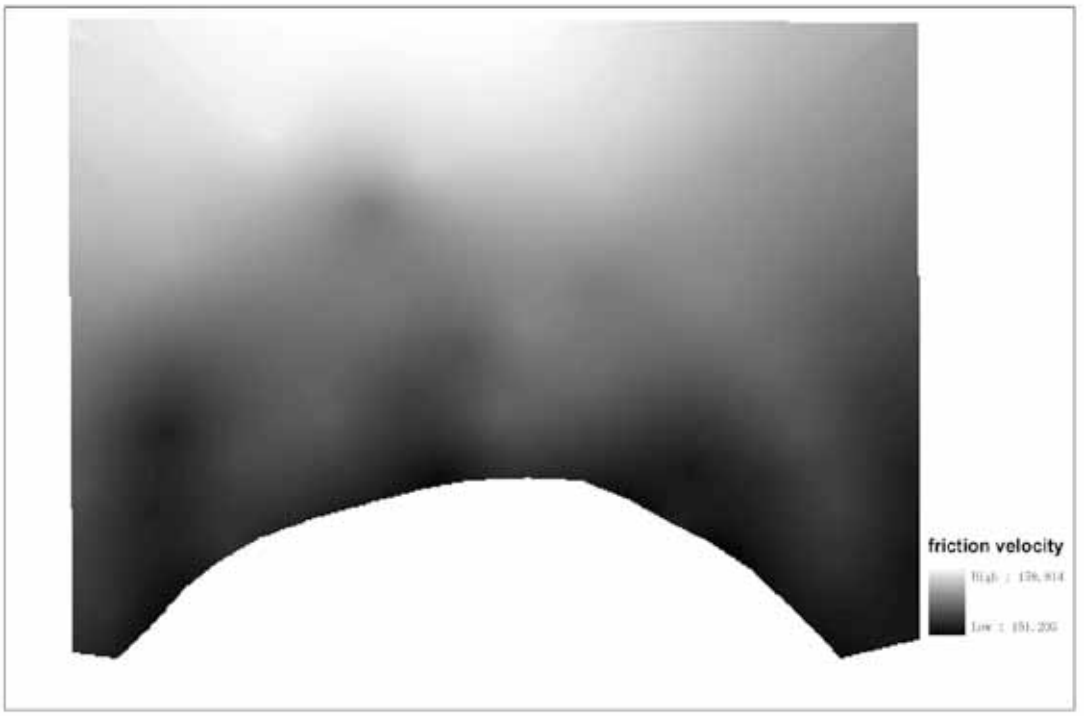

Fig. 4. Distribution of friction velocity above the surface of barchan dune

3.3.2. Wind velocity data pracessing

First, we normalized the wind velocity (v'_{ixy}) using the reference velocity (v_i) recorded at the same time:

$$v_{ixy} = v_1 \frac{v'_{ixy}}{v_i} \quad (6)$$

where, v_1 represents the reference velocity recorded at the first time.

Then, we used the Inverse Distance-Weighted method (IDW) to interpolate the wind velocities sample points. This approach uses the distance between the two points used for interpolation (the sample points) as the weight factor:

$$\hat{Z}(v_0) = \sum_{i=1}^{N} \lambda Z(v_i)_i \quad (7)$$

where, $\hat{Z}(v_0)$ is the predicted value of wind velocity at the point v_0 ; N is the number of sample points around the predicted point that is used in calculating the predicted value; λ is the weight factor, which decreases with increasing distance between the sample points and the predicted points. $Z(v_i)$ is the observed mean wind velocity in 10 minutes at sample point i.

This interpolation was performed using the Spatial Analyst module of the ArcGIS 9.2. In this way, we obtained a graph of wind velocity (m.s^{-1}) above the dune's surface, with 2×2 cm grids (Fig 3b).

3.4. Blown sand movement calculation

The friction velocity above a flat bed can be calculated by means of regression analysis, but the wind velocity profiles above the surface of dunes appear to be non-logarithmic in form [7, 26]. To overcome this problem, Mulliganamended Bagnold's friction velocity equation as follows [2, 26]:

$$V_* = (V_z - V_t)k / \ln(z / z'_0) \quad (8)$$

where, V_* denotes the friction velocity (cm.s^{-1}) near the bed; z represents the observed height above the bed (cm); k is Von Karman's constant (0.4); V_z (cm·s^{-1}) is the wind velocity at height z; and V_t is the threshold wind-velocity at height z'_0. Here, z'_0 represents the aerodynamic roughness length, which is commonly between 0.08 and 0.10 cm for dunes [2]; for the fine and very fine sand particles, we chose a value of 0.08 cm. V_t can calculated as follows:

$$V_t = 5.75A\sqrt{gd(\sigma - \rho)/\rho}\log(z_0^{'} / z_0) \quad (9)$$

where A is a constant (0.08); g is the acceleration due to gravity (980 cm·s^{-2}); d is the diameter (cm) of the sand particles; σ is the particle density of sand (from weighing the samples, an average value of 2.6 g·cm^{-3}); and ρ is the density of air (0.00129 g·cm^{-3}).

Page: 62

Because the drag stress and gravity acting on particles are in equilibrium under conditions of fluid movement, Bagnold proposed the following equation for the threshold friction velocity of sand, V_{*t} [2, 27]:

$$V_{*t} = A\sqrt{gd(\sigma - \rho)/\rho} \quad (10)$$

The most commonly used equations of sand flux are those proposed by Bagnold (1941), Lettau and Lettau, and Sørensen [2, 28, 29]. Respectively, these are:

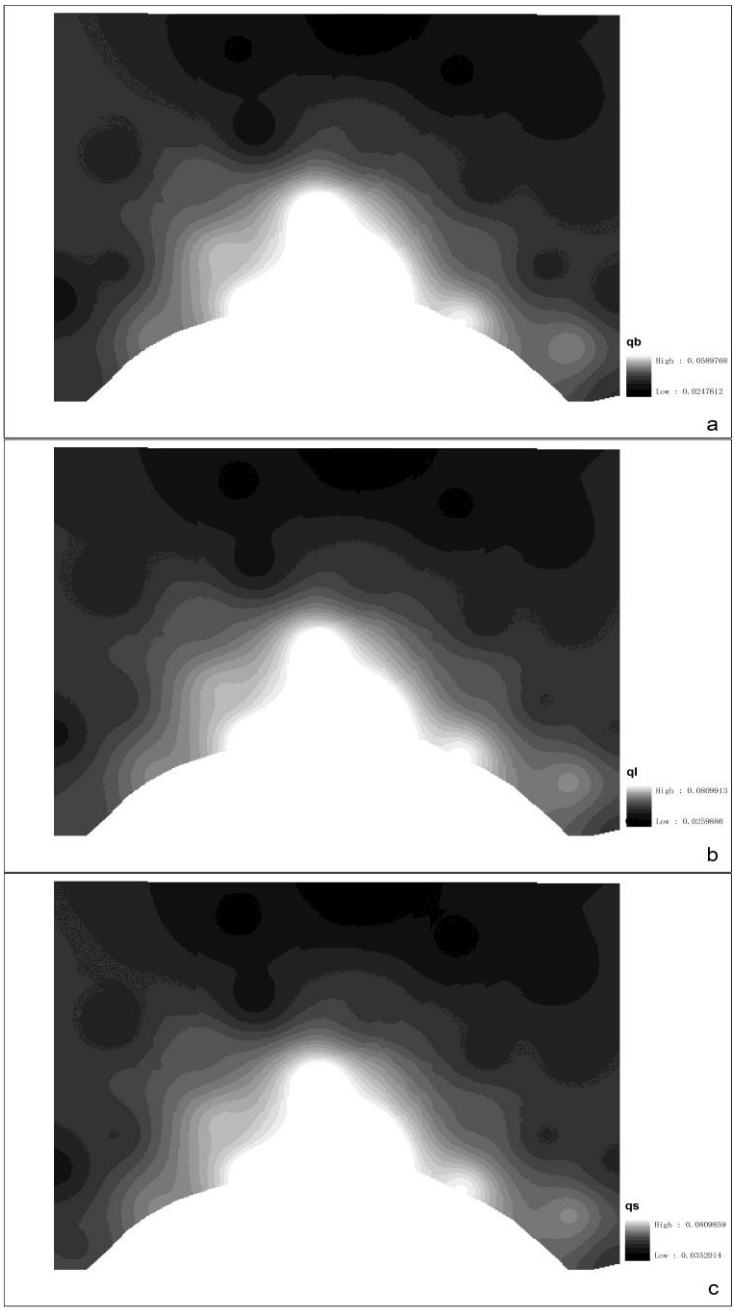

Fig. 5. Distribution of sand flux above the surface of the barchan dune (a. Bagnold model calculated results; b. Lettau's model calculated results; c. Sørensen's model calculated results)

$$q_B = C_B \frac{\rho}{g}\sqrt{\frac{d}{D}}V_*^3 \quad (11)$$

$$q_L = C_L \frac{\rho}{g}\sqrt{\frac{d}{D}}(V_* - V_{*_t})V_*^2 \quad (12)$$

$$q_S = C_S \frac{\rho}{g}\sqrt{\frac{d}{D}}V_*(V_* - V_{*_t})(V_* + 7.6V_{*_t} + 205) \quad (13)$$

where, D is the standard diameter (0.025 cm); q_B , q_L, and q_S (respectively) denote sand flux ($g.cm^{-1}.s^{-1}$) in the Bagnold, Lettau, and Sørensen models. C_B, C_L, and C_S are the corresponding constants (1.98, 4.1, and 0.4).

Based above equations, we got the blown sand movement parameters, which include aerodynamic roughness length, friction velocity, and sand flux (Fig 4 and Fig 5). By the way, all the calculation processes were performed in the grid module of ArcInfo Workstation 9.2 (ESRI).

4. Results analysis

4.1. Particle size and wind velocity

After processing the sand particle size data, we found that the fine and very fine sands were the main components (above 94%), with an average diameter of 0.01 cm. The sand particles were smallest at the slip face, and diameters increased moving from the slip face to the dune's foot. However, the mean particle diameter at the dune's foot (an average of 0.011 cm) was still smaller than the value for the flat ground surrounding the dune (an average of 0.013 cm). The particles at the noses of both horns were poorly sorted, with an average diameter of 0.0096 cm. The particles between the dunes exhibited the poorest sorting, with the largest diameters (reaching an average of 0.013 cm) (Fig 3a). This distribution was similar to those reported by Lancaster in the Namib Desert and Chen and Lei in the Taklimakan Desert [30, 31].

Perturbations caused by the topography cause the wind velocity to increase from the dune's foot to the dune's crest, and the wind velocity at both horns of the barchan is also higher than that at the dune's foot (Fig 3b).

There are two reasons for the increasing wind velocity from the dune's foot to the crest: first, the air flow is compressed by the stoss slope and this accelerates the air flow at greater heights; second, the free-stream wind velocity increases with height following approximately logarithmic equation within the boundary layer. When the air flow crosses the dune, for the dune's obstacle, it would separate and flows around the stoss slope. Moreover, the second flow that generated at the slip face will reattaches with the main air flow near the horns' noses. For the superposition of separated flow and second flow near the horns' noses, the wind velocity at the horns' noses is higher than that at the dune's foot.

4.2. Aerodynamic roughness length and friction velocity

We used the observed data set that collected at the same dune in 2007 to test our calculated aerodynamic roughness length and friction velocity. This data set has 4 observed points (dune's foot, dune's crest, and the noses of two horns), and at every point we got 20 wind profile data. Based on the

equation (1) proposed by Bagnold [2], we used this data set to calculate the aerodynamic roughness length and friction velocity by the method of least square.

$$\frac{V_z}{V_*} = \frac{1}{k}\ln(\frac{z-d'}{z_0'}) \tag{14}$$

where, d' denote the zero plane displacement can be assumed as 0. Then, we got the aerodynamic roughness length and friction velocity values.

The simulated values were evaluated by the deviation (R_e). The deviation values are given by the following equation [32] is defined as:

$$R_e = \left(\frac{P_i - O_i}{O_i}\right) \times 100\% \tag{15}$$

where， O_i and P_i are the observed and predicted values for the ith pair. The smaller the absolute value of R_e is, the closer simulated values are observed values.

In this paper, we used the data set that observed in 2007 as the observed values, and equation (14) calculated values as predicted values. Used equation (15), we got the deviations between the observed values and the predicted value (table 1).

Table 1 Deviations between the observed and predicted values above the different positions of the barchans

Positions	Observed values		Predicted values		R_e (%)	
	z_0'(cm)	V_* (cm/s)	z_0'(cm)	V_* (cm/s)	z_0'	V_*
Dune's foot	0.1224	170.321	0.08	159.755	34.64	-6.20
Dune's crest	0.0734	149.331	0.08	152.645	-9.00	2.22
Left horn's nose	0.1132	160.795	0.08	153.410	29.33	-4.59
Right horn's nose	0.1049	159.356	0.08	152.756	23.74	-4.14

As the table 1 showed, the predicted values are all satisfied and the deviations R_e between the observed and predicted values are all smaller than 35%. The table also showed the deviations of friction velocity are smaller than that of aerodynamic roughness length. The reason for this phenomenon is that we assumed the aerodynamic roughness length above the dune's surface as 0.08 cm in the simulation process. However, for the different particle size and characters of air flow above the different positions, the aerodynamic roughness length is not a constant. And the observed values also showed, the aerodynamic roughness length is biggest at the dune's foot and smallest at the dune's crest. For this reason, the simulated result of aerodynamic roughness length is not enough accurately.

We also found the friction velocity is also biggest at the dune's foot and smallest at dune's crest, and its distribution is same with the aerodynamic roughness length. To realize this question, we transformed equation (1), and we got the following equation:

$$V_* = \frac{V_z \mathrm{k}}{\ln(\mathrm{z}-d) - \ln z_0'} \tag{16}$$

Equation (16) showed the friction velocity is a monotonic function of aerodynamic roughness length. Hence, they have the same distributed trend at the dune's surface.

4.3. Sand flux

Figure 5 shows that the sand flux calculated by these models were all lowest at the foot of the dune, and increased with the height along the stoss slope, reaching a maximum at the crest of the dune. Moving sideways along the face of the dune, the sand flux increased from the dune's foot towards both horns, and increased moving upwards along the ridge line from the horns.

The distribution of the sand flux was essentially identical to that of wind velocity (Fig 3b), and the opposite of the distributrition of sand grain diameters (Fig 3a). There are two main reasons for this result: (1) During the evolution of the dune, the fine sands at the foot of the dune are blown away and deposited on the stoss slope and the crest. The particles that remain at the dune's foot are primarily coarse sands. This process depletes the supply of wind-transportable materials at the source. Hence, only limited sand flux develops at the foot of the dune. Moving towards the crest from the foot and both horns of the dune, the sand grain diameter gradually decreases, the sand source available for transport by the wind gradually increases, and the sand flux increases towards saturation. (2) The wind velocity decreases abruptly at the foot of the dune, and then increases along the dune's edge and the stoss slope, as the air flows across the dune. The following relationship holds:

$$\tau = \rho V_*^2 \qquad (17)$$

where, τ represents the shear stress of the air flow blowed over the dune. distribution of shear stress, which is the main stress responsible for saltation of particles, is identical to the distribution of wind velocity.

We summarized the predicted values provided by the three models and the observed values of sand flux at the five positions of the barchan dune (table 2). In this table, we can saw that these three models predicted results are all satisfied and the deviations are all lower than 30%. For didn't consider the threshold friction velocity, Bagnold model are worse than the others, and the deviation of Bagnold model are all bigger than 15%. The predicted results also revealed that the predicted results at the dune's foot are all not enough precisely. We analysed the reasons for this result, it caused by the unsaturated sand flux at the dune's foot, and these three models are all based on the theory of saturated sand flux. For the complex air flow at the noses of two horns, the predicted results at these places are not enough good. We simulated the air flow at these places used the software of FLUENT 6.0, and found the results is not enough exactly. We considered that we not fully understand the mechanism of unsaturated sand flux at the dune's foot and the air flow at the noses of two horns in present, so the simulated results at these places are not good enough.

Table 2. The predicted values provided by the three models and the actual measured values

Dune's positions	Predicted sand flux			Observed sand flux	Re (%)		
	Bagnold's model	Lettau's model	Sørensen's model		Bagnold's model	Lettau's model	Sørensen's model
Dune's foot	0.0247	0.0260	0.0325	0.0304	-18.75	-14.4737	6.907895
Middle of the stoss slope	0.0472	0.0617	0.0664	0.0655	-27.9389	-5.80153	1.374046
Dune's crest	0.0590	0.0810	0.0810	0.0794	-25.6927	2.015113	2.015113

Lift horn	0.0344	0.0425	0.0500	0.0476	-27.7311	-10.7143	5.042017
Right horn	0.0334	0.0414	0.0488	0.0451	-25.9424	-8.20399	8.203991

5. Conclusions

In recently years, new technology such as remote sensing and GIS were used in the research of blown sand movement. Ahmedou et al observed the sand flux and barchan dunes migration in Marritania, and found that the sand flux at the crest was about 3 times greater than the interdune mass transport rate, and the later followed the Sørensen law [18]. Daniell and Hughes got the morphology and sediment of subaqueous sand bank by Landsat data and multibeam sonar technology [19]. Vermeesch and Drake studied the relationship between dunes celerity and sand flux used ASTER satellite images in Chad [17]. Necsoiu et al quantified the subtle rate of dunes migration and evolution in Alaska used Co-registration of Optically Sensed Images and Correlation (COSI-Corr) technique [20]. However, these research were all emphasise on the dunes migration and sand flux in a vast region, and had no idear on how does the sand flux change above the different positions of a single barchan. In present study, we obtained the distribution of particle sizes, wind velocities, and sand flux above the surface of a barchan dune, and complemented the shortage of those research mentioned above. This approach also can overcome the problem of inadequate representation of the whole dune that is inherent in sampling at fixed points in the traditional method. This approach provides a useful new tool for research on aeolian process.

Based on the deviations between the blown sand movement parameters predicted and the measured values (Table 1 and Table 2), all the predicted results are all satisfied and the deviations are all below 35%. For the aerodynamic roughness length and friction velocity, the predicted results of aerodynamic roughness length are worse than that of friction velocity for we used the constantly aerodynamic roughness length. While, for the sand flux, the Bagnold model's simulated results are worse than the others models simulated results on the whole for it not considered the threshold friction velocity.

The results predicted by Lettau's model and Sørensen's model revealed the predicted results at the dune's foot are not enough precisely. We considered it caused by the unsaturated sand flux generated at this place. In present, the unsaturated sand flux is a difficult problem that perplexed many scholars. To resolve the problem of unsaturated sand flux simulation, we should develop a more precise model based on the saltation mechanisms of sand. Sauermann et al. proposed a continuum saltation model based on the physical mechanisms of saltation. Their model solved the problem of unsaturated sand flux, and reduced the number of calculations compared to a numerical simulation [10]. Unfortunately, the model required three phenomenological parameters that are very difficult to determine, which makes it difficult to use this model to predict sand fluxes. Developing a simple but still precise model of sand flux will be the subject of our future research.

We also found the air flow at the noses of two horns is very complex for the reattachment of second flow and separated flow. We simulated it used the software of FLUENT 6.0. However, the simulated result is not satisfied. To fully understand the characters of air flow at the noses two horns, we must do enough wind tunnel experiments and field observation. I think it will be one of our next work.

Acknowledgements

This work was supported by the National Major Fundamental Research Program of China (Grant No. 2011CB403306), the National Natural Science Foundation of China (No. 40571015), and the Knowledge Innovation Program of the Chinese Academy of Sciences (Grant No. KZCX1-YW-08-02).

References

[1] Han ZW, Dong ZB, Wang T, Chen GT, Yan CZ, Yao ZY. The observing and research of sand movement features in Taklimakan Desert. *Scientia Sinical (earth)* 2003; **33**: 255-63(in chinese).

[2] Bagnold RA. *The Physics of Blown Sand and Desert Dunes.* London: Chapman and Hall; 1941.

[3] Tsoar H. Profile analysis of sand dunes and their steady state significance. *Geogr. Ann. A* 1985; **67**: 45-59.

[4] Lancaster N. Reply: Variation in wind velocity and sand transport on the windward flanks of desert sand dunes. *Sedimentology* 1987; **34**: 511-20.

[5] Lancaster N. Dune morphology and dynamics. In: Abrahams, A. D. (ed). *Geomorphology of Desert Environments*, London: Chapman and Hill; 1994, p. 417-505.

[6] Burkinshaw JR, Llenberget WK, Rust LC. Wind-speed profile over a reversing transverse dune. K. Pye (ed). The dynamics and Environmental Context of Aeolian Sedimentary Systems. *Spe. Pub. Geol. Soc.* 1993; **72**: 25-36.

[7] Wiggs GFS. Desert dune dynamics and the evaluation of shear velocity: an integrated approach. *Geological Society*. London: Special Publications; 1993.

[8] McKenna Neuman C, Lancaster N, Nickling WG. Relations between dune morphology, air flow, and sediment flux on reversing dunes, Silver Peak, Nevada. *Sedimentology* 1997; **44**: 1103-14.

[9] Stam JMT. On the modeling of two-dimensional aeolian dunes. *Sedimentology* 1997; **44**: 127-41.

[10] Sauermann G, Kroy K, Herrmann HJ. A continuum saltation model for sand dunes. *Phy. Rev. E* 2001; **64**: 1-11.

[11] Sauermann G, Andrade JS, Maia LP, Costa UMS, Araujo AD, Herrmann HJ. Wind velocity and sand transport on a barchan dune. *Geomorphology* 2003; **54**: 245-55.

[12] Fryberger S, Dean G. Dune forms and wind regime, in A Study of Global Sand Sea, edited by E. Mckee, U.S. *Geol. Sury. Prof. Pap.*;1979, p.137-72.

[13] Zhu ZD, Zhao XL, Ling,YQ. *Engineering of blown sand control*. Beijing: Environment Science Press; 1998 (in Chinses).

[14] Livingstone I, Warren, A. *Aeolian geomorphology: an introduction*. Landon: Addison Wesley Longman Limited; 1996.

[15] Helen MR., Michele LC. ming climbing dune formation in southwestern Niger: fluvio-eolian interactions and the role of sand supply. *Quaternary Sci. Rev.* 2003; **22**: 1059-65.

[16] Dong ZB, Wang XM, Chen GT. Monitoring sand dune adance in the Taklimakan Desert. *Geomorphology* 2000; **35**: 219-31.

[17] Vermeesch P and Drake N. Remotely sensed dune celerity and sand flux measurements of the world's fastest barchans (Bodélé, Chad). *Geophy.l Res. Lett.* 2000; **35**: L24404, doi:10.1029/2008GL035921.

[18] Ahmedou DO, Mahfoudh AO, Dupont P, Moctar AO, Valance A, Rasmussen KR. Barchan dune mobility in Mauritania related to dune and interdune sand fuxes. *J. Geophy. Res*. 2007; **112**: F02016, doi: 10.1029/2006JF000500.

[19] Daniell JJ, Hughes M. The morphology of barchan-shaped and banks from western Torres Strait, northern Australia. *Sediment. Geol.* 2007; **202**: 638-52.

[20] Necsoiu M, Leprince S, Hooper DM, Dinwiddie CL, McGinnis RN, Walter GR. Monitoring migration rates of an active subarctic dune field using optical imagery. *Remote Sens. Envir.* 2009; **113**: 2441-7.

[21] Lancaster N, Nikling WC, McKenna Neuman KC, Wyatt VE. Sediment flux and airflow on the stoss slope of a barchan dune. *Geomorphology* 1996; **17**: 47-56.

[22] Nickling WC, McKenna NC. Recent investigations of airflow and sediment transport over desert dunes. In: Goudie A S, Livingstone I, Stokes S, eds. *Aeolian Environments, Sediments and Landforms*, Chichester: Wiley; 2000, p.15-47.

[23] Mamtimin A, Yang Q, Ghajigul S, Huo W, Gong Q. Microclimate effect of protective forest system in middle Taklimakan desert oil field. 2005; **25**: 535-40 (in chinese).

[24] Zhang CL, Hao QZ, Zou XY, Yan P. Response of morphology and deposits to surface flow on windward slope of barchans dunes. *J. Des. Res.* 1999; **19**: 359-64 (in Chinses).

[25] Hunt JRC, Leibovich S, Richard KJ. Turbulent wind flow over smooth hills. *Quarterly J. Royal Meteo. Soc.*1988; **114**: 1435-70.

[26] Mulligan KR. Velocity profiles measured on the windward slope of a transverse dune. *Earth Surf. Proc. Land.* 1988; **13**: 573-82.

[27] Wu Z. *Geomorphology of wind-drift sands and their controlled engineering*. Beijing: Science Press; 2003 (in Chinses).

[28] Lettau K, Lettau H. Experimental and micrometeorological field studies of dune migration. In: Lettau, H.H, Lettau, K. (Eds.), *Exploring the World's Driest Climate*. Center for Climatic Research: University of Madison-Wisconsin; 1978, p.110-47.

[29] Sørensen M. An analytic model of wind-blown sand transport. *Acta Mech. Suppl.* 1991; **1**: 67-81.

[30] Lancaster N.. T*he Namib Sand Sea: Dune forms, processes and sediments*. Rotterdam: A. A. Balkema; 1989.

[31] Chen WN, Lei JQ. The particle size types of barchan dunes different sections in Taklimakan Desert. *J. Arid Land Resou. Envir.* 1992; **6**: 101-8 (in Chinese).

[32] Yen BC. Criteria for evaluation of watershed models. *J. Irrig. Drain. E. ASCE* 1993; **119**: 429-42.